A 50 GHz GaAs FET MIC Transmitter/Receiver Using Hermetic Miniature Probe Transitions

KOICHI OGAWA, TOSHIO ISHIZAKI, KOJI HASHIMOTO, MAKOTO SAKAKURA, AND TOMOKI UWANO, MEMBER, IEEE

Abstract—**A very compact 50 GHz band transmitter/receiver for a video link has been developed. The RF assemblies in the system consist of 25/50 GHz frequency doublers, a 25 GHz DRO, and a 25 GHz FM modulator. The circuits make extensive use of MIC technology where the active elements used are all GaAs FET's. GaAs FET frequency doublers exhibited a minimum conversion loss of 2.6 dB and a maximum output power of 11 dBm. A 25 GHz FM modulator which was highly frequency stabilized by a dielectric resonator was obtained. Newly developed miniature probe microstrip-to-waveguide transitions permit the MIC assemblies to be installed compactly in hermetically sealed packages. Design considerations and experimental results of the transition are presented. With these technologies, a transmitting power of 10 dBm and a receiver noise figure of 13 dB were obtained.**

I. Introduction

STUDIES ON low-cost, compact, lightweight millimeter-wave systems using planar hybrid integrated circuit technologies have been reported in the past few years [1]–[4]. For millimeter-wave communication systems, of particular interest is the development of frequency-stable and inexpensive signal sources. The most commonly used devices to generate millimeter-wave signals are the two-terminal devices such as Gunn and IMPATT diodes [1]–[4]. However, oscillators with these active devices have certain drawbacks, such as poor dc-to-RF efficiency, which causes high-temperature operation, and since they are usually packaged in capsules it is difficult to adapt them for microwave integrated circuits (MIC's).

In this paper we present a very compact 50 GHz band transmitter/receiver where GaAs FET frequency doublers are used to multiply a 25 GHz signal into a 50 GHz signal. The RF assemblies in the system make extensive use of MIC technology where the active elements used are all GaAs FET's of chip form instead of two-terminal devices. The use of GaAs FET's leads to an inexpensive millimeter-wave communication system because of easy circuit adjustment due to the excellent and stable performance.

The system also has newly developed miniature probe microstrip-to-waveguide transitions which permit the MIC assemblies to be installed compactly in hermetically sealed packages. Although several kinds of transitions using finline [5], stripline probe [1], [3], and ridged waveguide [6] have been employed in millimeter-wave systems, it is difficult to realize these transitions in a hermetic structure. GaAs FET's and other three-terminal devices such as HEMT's are generally used in chip form in the millimeter-wave frequency range to avoid various parasitic impedances associated with the device package, and these chips need to avoid exposure to the atmosphere to achieve high reliability of the system for practical applications. We tried to use a coaxial miniature probe type transition in a hermetic structure which had been used at lower frequencies [7], [8] up to the 50 GHz band and good results were obtained.

The following sections provide an outline of the equipment, the design considerations, and experimental results of the microstrip-to-waveguide transition and those of various MIC components.

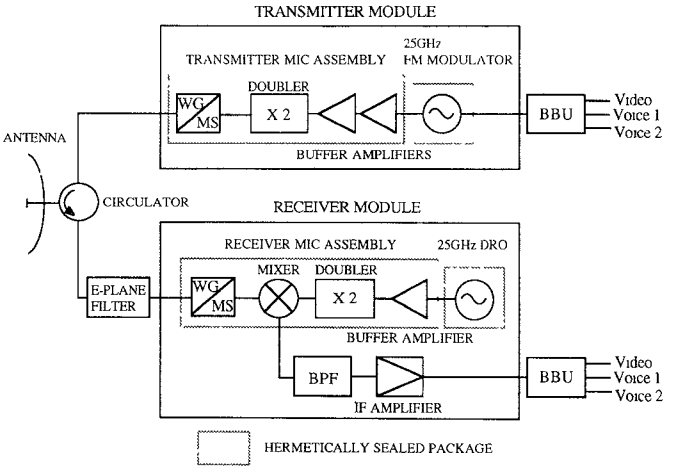

Fig. 1. Block diagram of the 50 GHz transmitter/receiver. BPF: bandpass filter; WG/MS: waveguide-to-microstrip transition; BBU: baseband unit.

II. System Configuration

A block diagram of the 50 GHz transmitter/receiver is shown in Fig. 1. The system consists of four major parts: 1) antenna and waveguide components; 2) transmitter module; 3) receiver module; and 4) baseband units. The transmitter module consists of a transmitter MIC assembly

Manuscript received December 8, 1988; revised April 12, 1989.

The authors are with the Development Research Laboratory, Matsushita Electric Industrial Company, Ltd., 1006, Kadoma, Osaka, 571 Japan.

IEEE Log Number 8928994

0018-9480/89/0900-1434$01.00 ©1989 IEEE

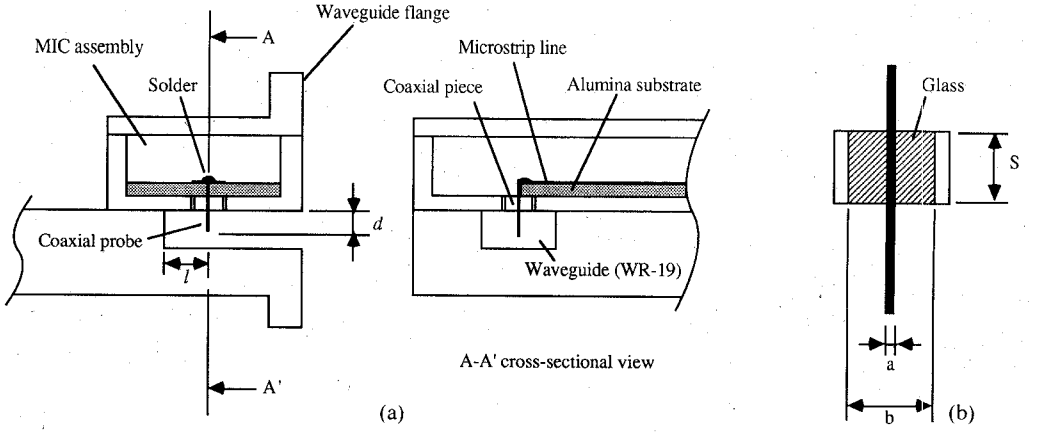

Fig. 2. Structure of the microstrip-to-waveguide transition. (a) Cross-sectional view. (b) Cross-sectional view of the coaxial piece.

and a 25 GHz FM modulator. The receiver module consists of a receiver MIC assembly, a 25 GHz DRO, and an IF amplifier. These are installed in hermetically sealed packages. An *E*-plane waveguide bandpass filter is used in the receiver input to suppress image signals and the local signal emission. The antenna is of the Cassegrain type with a diameter of 400 mm.

III. Microstrip-to-Waveguide Transition

The structure of the microstrip-to-waveguide transition is shown in Fig. 2. The transition consists of a miniature coaxial probe located at the center of the *H*-plane wall of a rectangular waveguide (WR-19), with its length d and distance l from the waveguide short. The probe is a part of the coaxial piece shown in Fig. 2(b) and this coaxial piece is embedded into the bottom base of the case of an MIC assembly and then soldered to form the coaxial probe. The inner conductor is connected to a 50 Ω microstrip line by soldering. The alumina substrate has a relative permittivity of 9.7 and a thickness of 0.2 mm. The glass filling in the coaxial piece has a relative permittivity of 5 and a loss tangent of 30×10^{-4} at 1 MHz. The characteristic impedance Z_0 and the approximate cutoff frequency f_c of a TE_{11} mode in a coaxial transmission line are given by the equations

$$Z_0 = \frac{60}{\sqrt{\epsilon_r}} \ln \frac{b}{a} \tag{1}$$

$$f_c = \frac{2c}{\pi(a+b)\sqrt{\epsilon_r}} \tag{2}$$

where ϵ_r is the relative permittivity of the glass and c is the velocity of light in free space [9]. It is obvious that the small size coaxial piece shows good electrical performance but it must have practical dimensions. Here, the coaxial piece is designed to have a characteristic impedance of 50 Ω and a cutoff frequency of 60 GHz. The dimensions of the structure were determined to be $a = 0.19$ mm and $b = 1.2$ mm.

Fig. 3 shows the equivalent circuit of the microstrip-to-waveguide transition, where Z_p represents the impedance

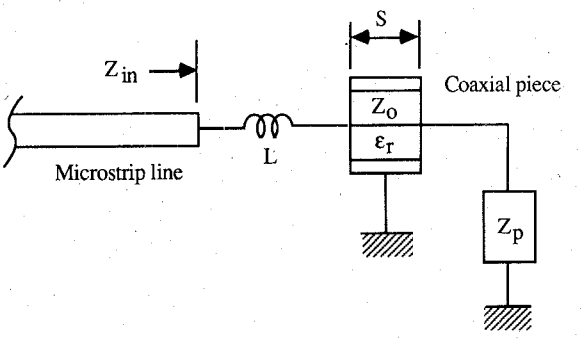

Fig. 3. Equivalent circuit of the microstrip-to-waveguide transition. Z_p: impedance of the probe; Z_0: characteristic impedance of the coaxial piece; ϵ_r: relative permittivity of the glass; L: discontinuity between the coaxial probe and the microstrip line.

of the probe. Discontinuity between the coaxial probe and the microstrip line is represented by L. The open-end effect of a microstrip line is ignored for simplicity of analysis. The impedance Z_{in} looking at L from the open end of the microstrip line is obtained as

$$Z_{in} = j\omega L + \frac{1+\Gamma_T e^{-j2\beta s}}{1-\Gamma_T e^{-j2\beta s}} Z_0 \tag{3}$$

where

$$\Gamma_T = \frac{Z_p - Z_0}{Z_p + Z_0} \qquad \beta = \frac{2\pi\sqrt{\epsilon_r}}{\lambda_0}$$

where λ_0 is the free-space wavelength. The calculated input impedance Z_{in} of the transition is shown in Fig. 4, where the probe impedances Z_p are calculated from the equations given by Collin [10]. The probe geometries (l, d) were selected so that Z_p becomes capacitive to cancel the inductance L at 50 GHz. The value L is estimated to be 0.1 nH from its physical length of 0.2 mm.

Fig. 5 shows the experimental results of the transition return loss and insertion loss, together with the calculated return loss of Z_{in} shown in Fig. 4. The experiment was made by connecting the probe transition under test to the ridged waveguide transition [6] at the output. The return loss of more than 15 dB was obtained over the frequency

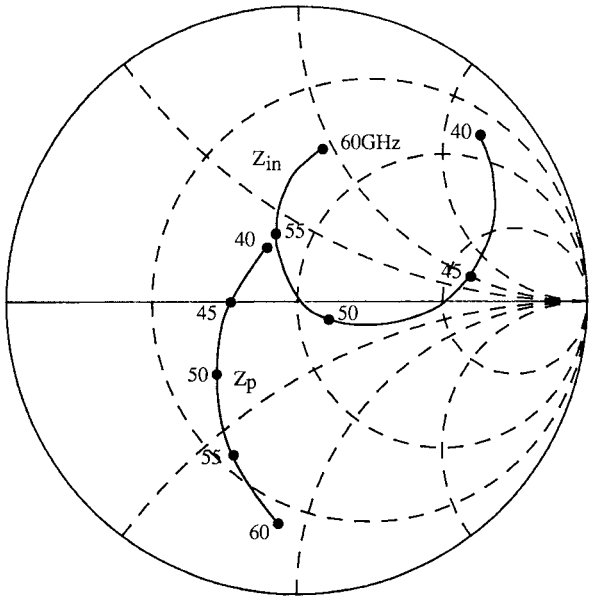

Fig. 4. Calculated input impedance Z_{in} of the microstrip-to-waveguide transition, where $a = 0.19$ mm, $b = 1.2$ mm, $l = 1.1$ mm, $d = 1.2$ mm, $s = 1$ mm, $\epsilon_r = 5$, $Z_0 = 50\ \Omega$, and $L = 0.1$ nH. The probe impedances Z_p are calculated from the equations given by Collin [10]. The normalized impedance is 50 Ω.

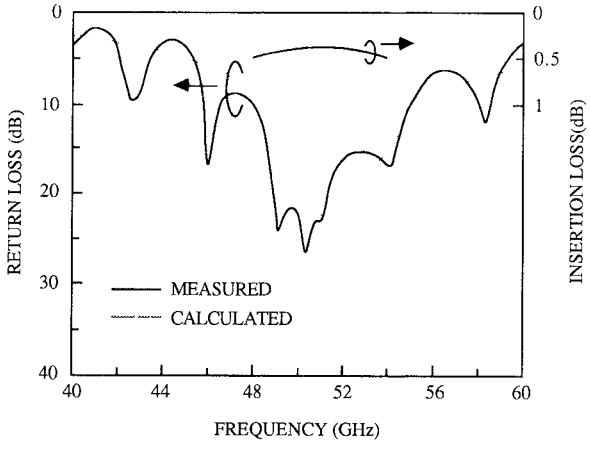

Fig. 5. Measured return loss and insertion loss of the microstrip-to-waveguide transition (solid line), where $a = 0.19$ mm, $b = 1.2$ mm, $l = 1.1$ mm, $d = 1.2$ mm, $s = 1$ mm, $\epsilon_r = 5$, $Z_0 = 50\ \Omega$, and $L = 0.1$ nH. The dotted line represents the calculated return loss of Z_{in} shown in Fig. 4.

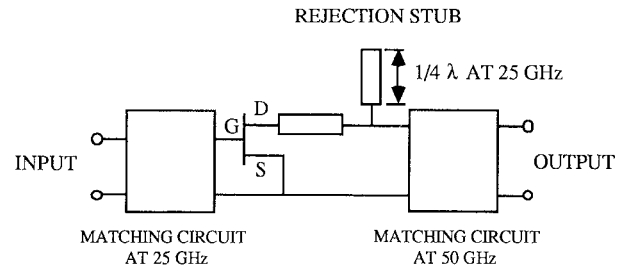

Fig. 6. Circuit of the 25/50 GHz frequency doubler.

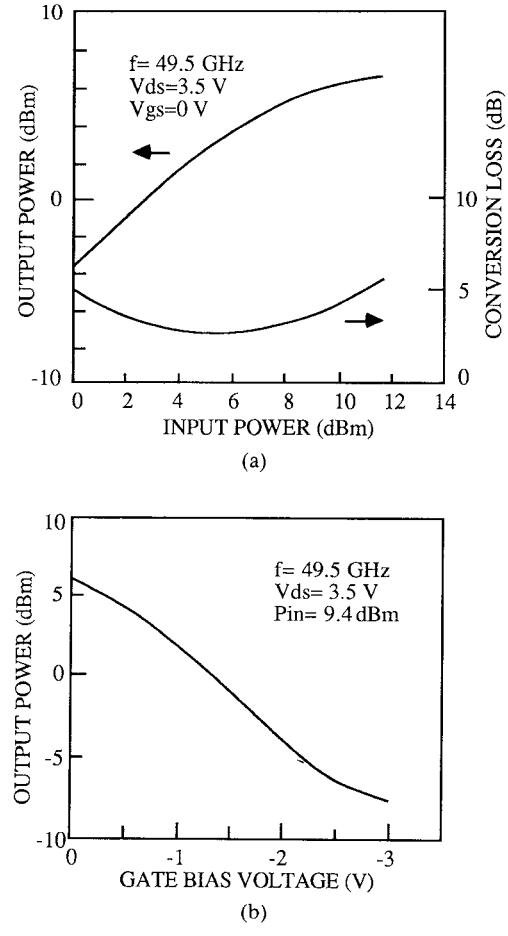

Fig. 7. Performance of the frequency doubler with a small-signal FET of 0.5 μm gate length and 150 μm gate width. (a) Input–output power characteristics. (b) Gate bias voltage dependence.

range 48–54 GHz. The insertion loss of the probe transition was less than 0.5 dB in the same frequency range.

IV. MIC Components

A. 25/50 GHz Frequency Doubler

Fig. 6 shows the circuit configuration of the 25/50 GHz frequency doubler. It has an input matching circuit for the input frequency of 25 GHz, a GaAs FET in a common-source configuration, a rejection stub for 25 GHz signal at the output port, and a 50 GHz output matching circuit. The rejection stub performs as a short circuit at the fundamental frequency and reflects the power to the FET. At 50 GHz, this stub does not influence the transmitting power because of its high impedance. The GaAs FET chip is mounted on a metal pedestal between two 0.2-mm-thick alumina substrates. Frequency doublers of this type have already been reported in the millimeter-wave frequency range below 40 GHz [11], [12]. In order to examine the feasibility of a GaAs FET frequency doubler operating at 50 GHz, two kinds of frequency doublers with a FET having a different gate width were tested. One used a so-called small-signal FET with a gate length of 0.5 μm and a gate width of 150 μm (Avantek AT-8041, $I_{dss} = 30$ mA, $V_p = -1.5$ V); the other used a medium power FET with a gate length of 0.5 μm and a gate width of 360 μm (Fujitsu FLR014XP, $I_{dss} = 80$ mA, $V_p = -3$ V).

Fig. 7 shows the performance of the frequency doubler with the small-signal FET, and Fig. 8 shows it with the

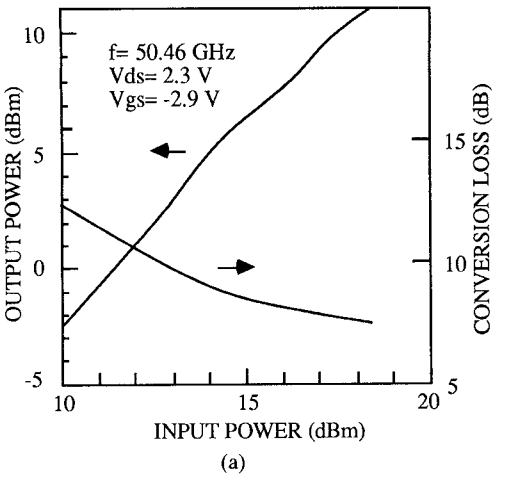

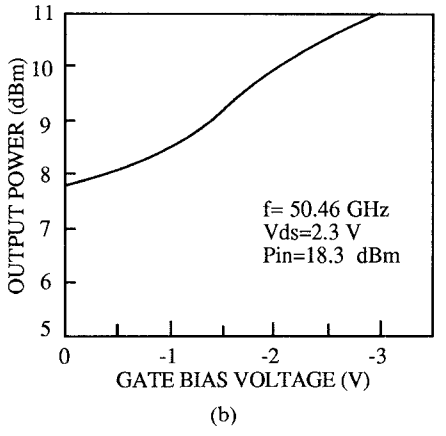

Fig. 8. Performance of the frequency doubler with a medium power FET of 0.5 μm gate length and 360 μm gate width. (a) Input–output power characteristics. (b) Gate bias voltage dependence.

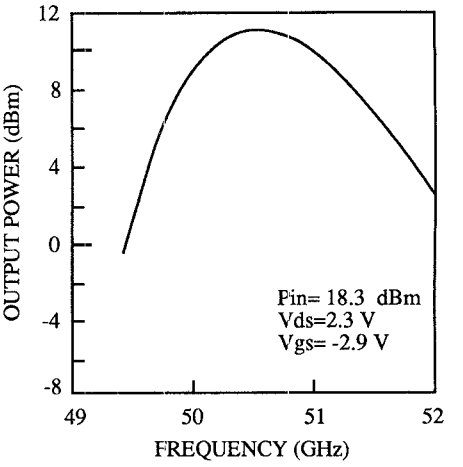

Fig. 9. Frequency response of the frequency doubler with a medium power FET of 0.5 μm gate length and 360 μm gate width.

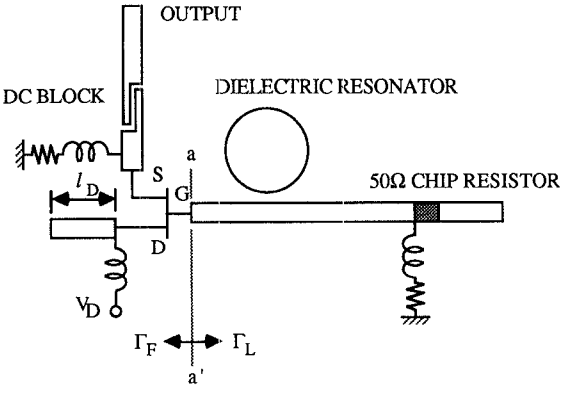

Fig. 10. Circuit of the 25 GHz DRO.

medium power FET. The experimental results show the performance at the gate and drain ports of the FET. It is learned from Fig. 7 that the minimum conversion loss of 2.6 dB was obtained at an input power level of 5.5 dBm, and Fig. 8 shows that the maximum output power of 11 dBm was obtained with an input power level of 18.3 dBm. Although the experiments were not performed beyond an input power of 18.3 dBm, greater output power can be expected in Fig. 8(a) with a lower conversion loss at higher input power. Both frequency doublers were stable, and no parasitic oscillation was observed during the experiments. The frequency doubler with the small-signal FET exhibits a small conversion loss and may be usable for the local oscillator source but it is not suitable for our particular system, which requires an output power of 10 dBm. The maximum output power for the medium power FET doubler was obtained when the gate bias was nearly at the pinch-off. The gate current was then 50 μA. This value is sufficiently small since it is known that a gate current over 100 μA causes a degradation of the reliability.

Fig. 9 shows the frequency characteristics of the doubler (360 μm gate width) at an input power of 18.3 dBm. The 1 dB bandwidth was approximately 0.7 GHz.

B. 25 GHz DRO

1) Oscillator Circuit: The oscillator circuit is shown schematically in Fig. 10. It is fabricated on a 0.3-mm-thick alumina substrate. The GaAs FET used here has a 0.5×600 μm gate (Fujitsu FLR024XV, $I_{dss} = 100$ mA, $V_p = -2$ V). The oscillator circuit is of the Colpitts type in a common-drain configuration with the source output port. The oscillator is stabilized by a $TE_{01\delta}$-mode dielectric resonator which is placed on the alumina substrate and magnetically coupled to the microstrip line with a 50 Ω load at the end. The dielectric resonator, made of a material system of $Ba(Zn_{1/3}Nb_{2/3})O_3$–$Ba(Zn_{1/3}Ta_{2/3})O_3$ [13], has an unloaded Q of 2000, a relative dielectric constant of 35, and a resonator-frequency temperature coefficient of +11 ppm/°C at 25 GHz. The cylindrical dielectric resonator is 2.8 mm in diameter and 0.8 mm in thickness. The metal disk with tuning screw is placed above the resonator to confine the electromagnetic field, which makes an unloaded Q large, and to adjust the resonant frequency.

2) Design Considerations: An oscillating condition for the oscillator in Fig. 10 is determined by the equation $|\Gamma_L| > 1/|\Gamma_F|$ and $\arg(\Gamma_L) = -\arg(\Gamma_F)$, where Γ_L is the reflection coefficient looking at the resonator from the reference plane (a–a'), and Γ_F is that of the GaAs FET including the load. Fig. 11 shows the calculated results of

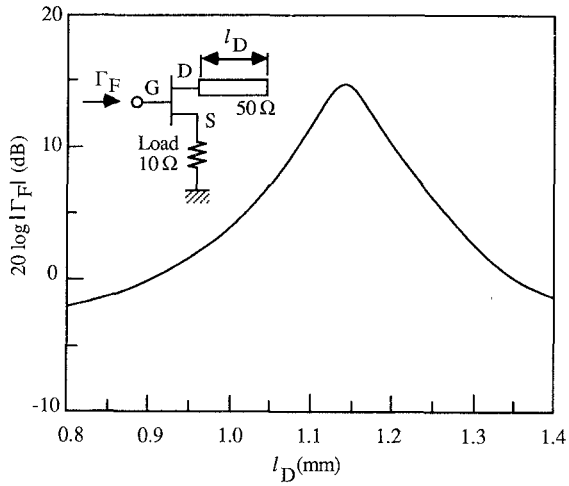

Fig. 11. Calculated reflection coefficient Γ_F with respect to the length of the open-circuited stub connected to the drain at 25 GHz.

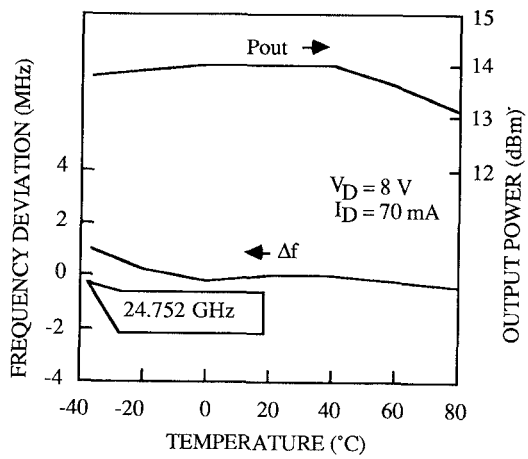

Fig. 12 Temperature characteristics of the 25 GHz DRO.

$|\Gamma_F|$ using the measured small-signal S parameters with respect to the length of the open-circuited stub connected to the drain. From Fig. 11, the length of the stub was determined to be 1.14 mm where $|\Gamma_F|$ has a maximum value.

Γ_L was experimentally determined by varying the coupling between the dielectric resonator and the microstrip line in order to satisfy the oscillating condition. Oscillator temperature drift was compensated by choosing the appropriate value of the temperature coefficient of the dielectric resonator and partly by optimizing Γ_L [14] and readjusting the stub length.

3) Experimental Results: Fig. 12 shows the measured results of the temperature characteristics of the DRO. In this case, the optimum length of the drain stub was approximately 0.95 mm. Average frequency stability of 0.2 ppm/°C was obtained over a temperature range from −20 to 60°C with a power output of more than 13.6 dBm at 24.75 GHz. The output power change was less than ±0.5 dB in the same temperature range. The voltage pushing figure of the DRO was typically 1 MHz/V at 20°C. Operating voltage and current were 8 V and 70 mA.

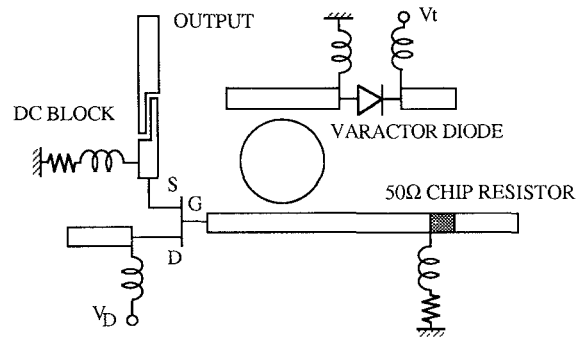

Fig. 13 Circuit of the 25 GHz FM modulator

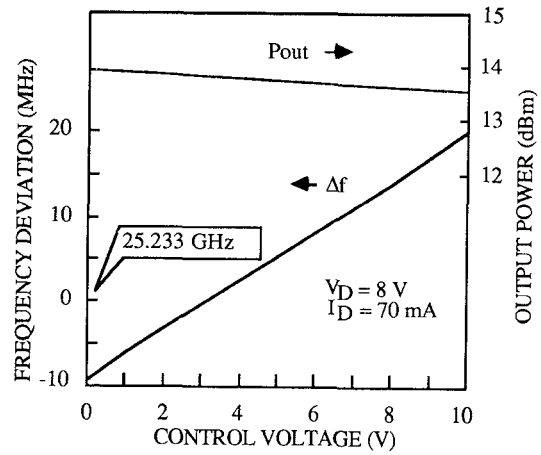

Fig. 14 Linearity performance of the 25 GHz FM modulator.

The oscillation efficiency $[P_{osc}/(V_D \times I_D)]$ was approximately 5 percent.

C. 25 GHz FM Modulator

Fig. 13 shows the circuit of the 25 GHz FM modulator. The modulator possesses the same kind of 25 GHz DRO as described above and a varactor-tuned parasitic microstrip line resonator. The dielectric resonator used has almost the same characteristics as that used in the DRO except for a resonant-frequency temperature coefficient of +22.5 ppm/°C. The varactor diode has a capacitance of 0.5 pF at a bias voltage of −4 V and a quality factor of 750 at 1 GHz (Alpha CVE7800). The varactor diode is inserted between a 3/4 wavelength open stub and a 1/4 wavelength open stub and connected to form a wavelength microstrip line resonator whose resonant frequency varies in accordance with the control voltage (V_t) of the varactor diode. Modulation linearity was adjusted by varying the coupling between the varactor diode and the dielectric resonator.

Fig. 14 shows the linearity performance of the FM modulator under the same dc power condition as in the 25 GHz DRO. The center oscillation frequency was 25.233 GHz and output power was more than 13.5 dBm. Modulation sensitivity was 2.8 MHz/V and modulation linearity was less than 2 percent in a deviation range of ±4 MHz. The temperature characteristics of the FM modulator are shown in Fig. 15. Output power of more than 13.2 dBm

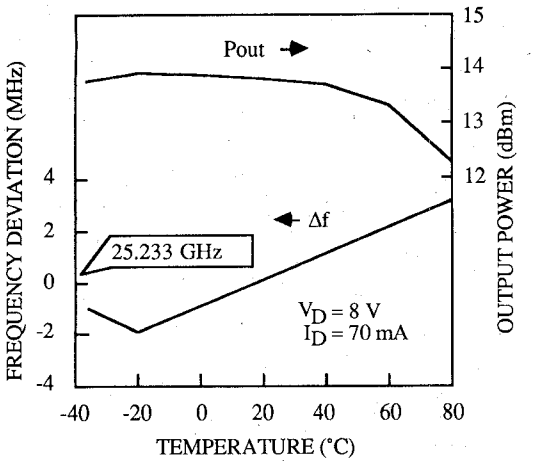

Fig. 15. Temperature characteristics of the 25 GHz FM modulator.

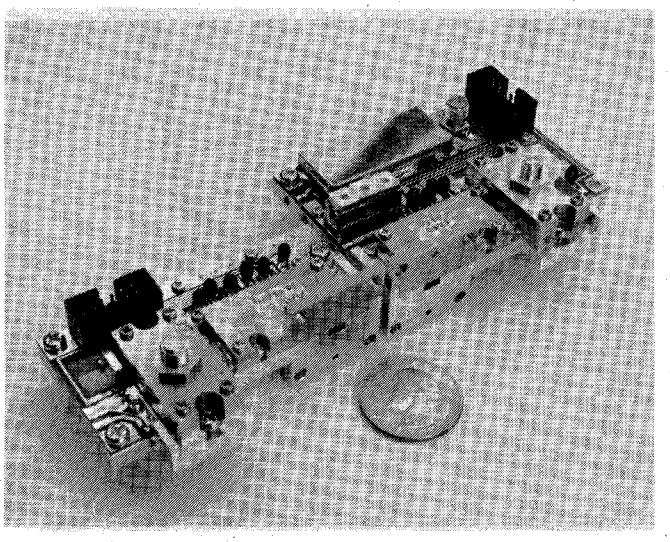

Fig. 16. External view of the transmitter module (left side) and the receiver module (right side).

and average frequency stability of 2 ppm/°C were obtained over the temperature range from −20 to 60°C.

D. Mixer and Buffer Amplifier

A conventional single balanced hybrid mixer is employed in the receiver where two silicon Schottky barrier beam-lead diodes are used. A typical conversion loss of 9 dB was obtained at 8 dBm local power.

Buffer amplifiers are used in both the transmitter and the receiver to supply sufficient input power to the frequency doublers and to minimize the frequency pulling effect on the 25 GHz DRO's. The single-stage amplifier in the receiver provided an output power of 17 dBm, and the two-stage amplifier in the transmitter provided an output power of 20 dBm to the doublers. Linear gains of the single-stage and the two-stage amplifier were 4 dB and 8 dB.

V. System Performance

Fig. 16 shows an external view of the transmitter and the receiver module. Alumina substrates are directly soldered to the bottom base of MIC assemblies or oscillator

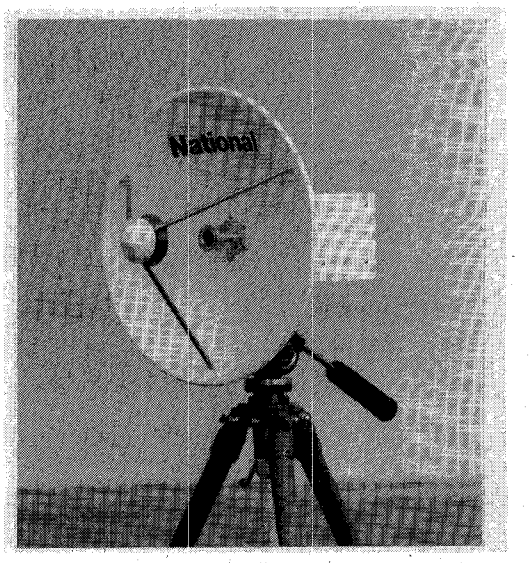

Fig. 17. External view of the transmitter/receiver equipment.

TABLE I
MAJOR CHARACTERISTICS OF THE 50 GHz TRANSMITTER/RECEIVER

Transmitting frequency	50.94 GHz
Receiving frequency	50.44 GHz
Transmitting power	10 dBm
Noise figure	13 dB
Frequency stability	± 100 pm (-20~ 60 °C)
Modulation	FM
Frequency deviation	16 MHz pp
Intermediate frequency	1040 MHz
IF bandwidth	27 MHz
Local oscillator leakage	-34 dBm
Spurious radiation	-46 dBm (at 76.41 GHz)
Video signal bandwidth	4 MHz
S/N (unweighted)	50 dB (at a receiving input of -50 dBm)
DG/DP	5% / 5°
Audio signal bandwidth	15 KHz

cases without a metal carrier to avoid connection losses due to imperfect electrical contact at the substrate ground conductor [2], [3]. This structure contributes to the realization of inexpensive and performance-stable millimeter-wave equipment because of a simple fabrication process and small circuit losses. Coaxial pieces used for the microstrip-to-waveguide transition described in Section III are also used as feedthroughs in the RF input and output ports for the 25 GHz DRO, the FM modulator, and the MIC assemblies. The coaxial piece used as a feedthrough showed a loss of 0.1 dB at 25 GHz. The 25 GHz DRO and

the FM modulator output were connected to the MIC assembly inputs by using short lengths of microstrip lines.

Fig. 17 shows the external view of the transmitter/receiver equipment, in which the baseband circuits and power supplies are also installed. The dimensions of the equipment are $120 \times 180 \times 230$ mm^3. A Cassegrain antenna has 43 dBi gain and 1° beamwidth. The voltage of a dc power supply is 12 V, and total dissipation power is 12 W. Table I summarizes the major characteristics of the system. A transmitting power of 10 dBm with a frequency stability of less than ± 100 ppm over the temperature range from -20 to 60°C and a receiver noise figure of 13 dB were obtained.

VI. Conclusion

A very compact 50 GHz band transmitter/receiver for a video link has been developed by using newly developed hermetic miniature probe microstrip-to-waveguide transitions and by making extensive use of GaAs FET MIC technology. The system contains 25/50 GHz frequency doublers, a 25 GHz DRO, and a 25 GHz FM modulator with excellent and stable performance. The complete hermetic sealing technology of the millimeter-wave MIC's presented in this paper contributes to the increase of reliability and thus will promote the practical use of GaAs FET's and HEMT's in their chip form in the millimeter-wave frequency range.

Acknowledgment

The authors wish to thank Dr. Y. Nagaoka and T. Tatsuzawa for supporting and encouraging this work. They also would like to acknowledge the efforts of Y. Tsujimoto for MIC processing.

References

[1] Y. Tokumitsu, M. Ishizaki, M. Iwakuni, and T. Saito, "50-GHz IC components using alumina substrates," *IEEE Trans. Microwave Theory Tech.*, vol. MTT-31, pp. 121–128, Feb. 1983.

[2] E. Hagihara, H. Ogawa, N. Imai, and M. Akaike, "A 26-GHz miniaturized MIC transmitter/receiver," *IEEE Trans. Microwave Theory Tech.*, vol. MTT-30, pp. 235–242, Mar. 1982.

[3] H. Ogawa, K. Yamamoto, and N. Imai, "A 26-GHz high-performance MIC transmitter/receiver for digital radio subscriber systems," *IEEE Trans. Microwave Theory Tech.*, vol. MTT-32, pp. 1551–1556, Dec. 1984.

[4] A. Grote and K. Chang, "60-GHz integrated-circuit high data rate quadriphase shift keying exciter and modulator," *IEEE Trans. Microwave Theory Tech.*, vol. MTT-32, pp. 1663–1667, Dec. 1984.

[5] M. Dydyk, "Shielded microstrip aids *V*-band receiver designs," *Microwaves*, pp. 77–82, Mar. 1982.

[6] K. Ogawa, T. Ishizaki, K. Hashimoto, M. Sakakura, and T. Uwano, "A 50-GHz compact communication system for video link fabricated in MIC," in *1988 IEEE MTT-S Int. Microwave Symp. Dig.*, pp. 1023–1026.

[7] K. Shibata *et al.*, "20 GHz-band low-noise HEMT amplifier," in *1986 IEEE MTT-S Int. Microwave Symp. Dig.*, pp. 75–78.

[8] M. Ishizaki *et al.*, "A 43 GHz-band balanced low-noise amplifier," in *1988 IEEE MTT-S Int. Microwave Symp. Dig.*, pp. 461–464.

[9] N. Marcuvitz, *Waveguide Handbook*. London: Peter Peregrinus, 1986, sec. 2.4.

[10] R. E. Collin, *Field Theory of Guided Waves*. New York: McGraw-Hill, 1960, ch. 7.

[11] R. Rauscher, "High-frequency doubler operation of GaAs field-effect transistors," *IEEE Trans. Microwave Theory Tech.*, vol MTT-31, pp. 462–473, June 1983.

[12] G. S. Dow and L. S. Rosenheck, "A new approach for mm-wave generation," *Microwave J.*, pp. 147–162, Sept. 1983.

[13] S. Kawashima, M. Nishida, I., Ueda, and H. Ouchi, "$Ba(Zn_{1/3}Nb_{2/3})O_3$ ceramics with low dielectric loss at microwave frequencies," *J. Amer. Ceram. Soc.*, vol. 66, no. 6, pp. 421–423, June 1983.

[14] T. Makino and A. Hashima, "A highly stabilized MIC Gunn oscillator using a dielectric resonator," *IEEE Trans. Microwave Theory Tech.*, vol MTT-27, pp. 633–638, July 1979.

Koichi Ogawa was born in Kyoto, Japan, on May 28, 1955. He received the B.S. and M.S. degrees in electrical engineering from Shizuoka University, Japan, in 1979 and 1981, respectively.

He joined Matsushita Electric Industrial Co., Ltd., Osaka, Japan, in 1981, and has been engaged in research and development work on microwave integrated circuits and satellite communication. He is presently engaged in research and development on millimeter-wave integrated circuits.

Mr. Ogawa is a member of the Institute of Electronics, Information and Communication Engineers of Japan.

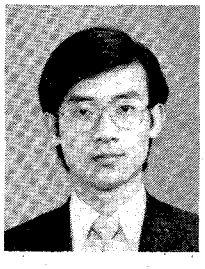

Toshio Ishizaki was born in Kagawa, Japan, on May 24, 1958. He received the B.S. and M.S. degrees in electrical engineering from Kyoto University, Japan, in 1981 and 1983, respectively.

He joined Matsushita Electric Industrial Co., Ltd., Osaka, Japan, in 1983, where he has been engaged in research and development work on microwave and millimeter-wave circuits and satellite communication systems.

Mr. Ishizaki is a member of the Institute of Electronics, Information and Communication Engineers of Japan.

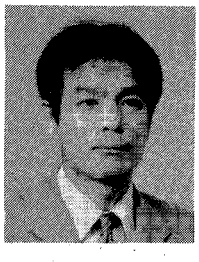

Koji Hashimoto was born in Osaka, Japan, on February 15, 1961. He graduated from Nara Technical College, Japan, in 1981.

He joined Matsushita Electric Industrial Co., Ltd., Osaka, Japan, in 1981, and has been engaged in the development of FM radio circuits. He is presently engaged in research and development work on microwave and millimeter-wave integrated circuits.

Mr. Hashimoto is a member of the Institute of Electronics, Information and Communication Engineers of Japan.

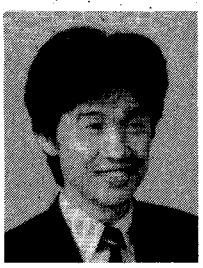

Makoto Sakakura was born in Fukuoka, Japan, on December 23, 1959. He received the B.S. and M.S. degrees in electrical engineering from Kyusyu University, Japan, in 1983 and 1985, respectively.

He joined Matsushita Electric Industrial Co., Ltd., Osaka, Japan, in 1985, and has been engaged in research and development work on microwave integrated circuits and satellite communication.

Mr. Sakakura is a member of the Institute of Electronics, Information and Communication Engineers of Japan.

Tomoki Uwano (M'87) was born in Toyama, Japan, on October 18, 1948. He received the B.S. degree from the Tokyo Institute of Technology in 1971.

Since 1971, he has been employed by the Matsushita Electric Industrial Co., Ltd, Osaka, Japan, where he has been engaged in research and development work on microwave and millimeter-wave circuitry and satellite communication. From April 1985 to December 1986, he was a Visiting Scholar in the Department of Electrical and Computer Engineering at the University of Texas at Austin.

Mr. Uwano is a member of the Institute of Electronics, Information and Communication Engineers of Japan.